

Direct Experimental Observation of the Tetrabromine Cluster Br₄ by Synchrotron Photoionization Mass Spectrometry

Rory McClish^[a] and Giovanni Meloni^{*[a, b]}

We present a first spectroscopic characterization of the homoatomic polyhalogen tetrabromine, Br₄, in the gas phase. Photolysis of CHBr₃ at 248 nm is used to generate atomic bromine radicals in a flow tube reactor. Resulting combination products are detected by photoionization mass spectrometry at the Advanced Light Source of the Lawrence Berkeley National Laboratory. Interpretation of the experimental mass spectra is

informed by calculated adiabatic ionization energies carried out at the CCSD(T)/aug-cc-pVTZ//M06-2X/aug-cc-pVTZ and CCSD(T)/aug-cc-pVTZ//cam-B3LYP/6-311++g** levels of theory. Tunable VUV synchrotron radiation enables the collection of the mass-selected photoionization spectra by which Br₄ is assigned using Franck-Condon simulations of a Br₂ dimer with a stretched tetrahedral geometry.

Introduction

Homopolyatomic halogen chemistry has a rich historical foundation since the late 18th century and continued interest today.^[1] Fundamental insights into such chemistry is driven by a wide range of phenomena. Polybromine crystals have use in superconducting materials, whereas atomic and molecular bromine have a significant role in climate cycles including ozone depletion.^[2] Although diatomic halogens have long been well characterized, this renewed interest expands to larger clusters, X_n, for n > 2.^[3] Triatomic clusters, X₃, have been spectroscopically characterized for X = Cl, Br, and I by X-ray crystallography and Raman spectroscopy.^[3c,4] Interaction of X₃ with the dimer, X₂, is found to form X₅ for X = Br, I.^[5] Clusters with n = 4 are more elusive. Gillespie *et al.*^[6] synthesized the diamagnetic I₄²⁺ in the solid state (while Brichall and Myers^[7] found it in solution) with a structure described by π*-π* overlap and having a square planar geometry. Additionally, Chance *et al.*^[8] conducted electric deflection studies on a set of halogen clusters and proposed that Br₄ is polar. Multiple theoretical investigations have worked to further propose the structure of Br₄. Schuster *et al.*^[9] conducted a DFT study of neutral and ionic polybromine clusters from n = 1-5 and proposed a L-shaped neutral Br₄ and a twisted Br₄⁺ with C_s and

C_i symmetry, respectively. However, Thanthiriwatte *et al.*^[10] included dispersion corrected DFT methods as well as *ab-initio* CCSD(T) to argue that Br₄⁺ has a planar D_{2h} symmetry. Long range intermolecular interactions are certainly expected to play a role, but thus far theory has not been able to be compared to experiment.

Photoionization mass spectrometry coupled to tunable VUV light offers a compelling opportunity to detect and characterize the tetratomic bromine cluster. The equilibrium structures of both neutral and cationic Br₄ is expected to determine the ionization energies with isomeric selectivity. Moreover, by tuning the photon energy of the ionizing synchrotron radiation over the first ionization potential of a species, the shape of the resultant photoionization (PI) spectrum is dependent on the photoionization cross section. The cross section itself is partially dependent on the transition between neutral and cation, thereby further reporting on the structure of a target. We herein present measurement of the Br₄⁺ cation through the use of photoionization mass spectrometry (PIMS) via tunable synchrotron radiation. Structural assignments are rationalized via quantum chemistry calculations and comparison of integrated theoretical photoelectron simulations.

Experimental and Computational Methods

Experiments were carried out at the Advanced Light Source (ALS) of Lawrence Berkeley National Laboratory. A more detailed explanation of the experimental technique is available and only a brief summary is given here.^[11] Dilute bromoform (CHBr₃, 1% in Ar) was flowed into a vertical 62 cm long quartz flow-tube reactor (~1 cm I.D.) and subsequently photolyzed by a pulsed KrF excimer laser at 248 nm fired at 10 Hz and 30 kV. The laser power was measured at 406 mJ/pulse and the measured power transmittance through the reactor tube was 17.5%. Resulting bromine atoms are produced via the multi-photon dissociation of CHBr₃. Estimating the number density of

[a] R. McClish, Prof. G. Meloni
Department of Chemistry
University of San Francisco
San Francisco, CA 94117, USA

[b] Prof. G. Meloni
Department of Biological and Chemical Sciences
New York Institute of Technology
Old Westbury, NY 11568, USA
E-mail: gmeloni@nyit.edu

© 2024 The Authors. ChemistryOpen published by Wiley-VCH GmbH. This is an open access article under the terms of the Creative Commons Attribution License, which permits use, distribution and reproduction in any medium, provided the original work is properly cited.

bromine radicals at this stage is unfeasible due to the five proposed photodissociation pathways of bromoform accessible in the UV region.^[12] Reaction species escape out sideways from the reactor via a 650 μm pinhole and the expansion is skimmed using a 1.5 mm diameter skimmer. The molecular beam is orthogonally intercepted by tunable synchrotron light stepped at 25 meV between 8.00–10.75 eV. A shift of +0.0272 eV based on known Xenon resonances is applied after calibration and all spectra are normalized to the measured VUV photocurrent. Additionally, ion-signals appearing post photolysis are background subtracted to show only the ion signal contribution after the excimer laser begins firing at $t_{\text{rxn}}=20$ ms. Photoionization occurs if the photon energy exceeds the ionization energy of a neutral species in the molecular beam. For a given ionization event, each photoion born from the molecular beam is subject to focusing by static electric fields onto a multi-channel plate detector (MCP). The resulting ion counts as a function of flight time thus compose a time-of-flight mass spectrum. The tunable synchrotron VUV light serves a crucial purpose for product characterization, as the collected ion signal is a function of mass, reaction time (determined by the triggering of a photolysis laser), and photon energy. Integrating over carefully selected mass and time bounds allows for plotting the ion signal as a function of photon energy to reveal a mass-selected photoionization (PI) spectrum. Bromine-containing peaks are quickly identified in the mass spectrum based on the 51/49 isotopic abundance between $^{79}\text{Br}/^{81}\text{Br}$. Furthermore, since the shape of the PI spectrum is dependent on the difference between the neutral and cationic structures, the spectral onset is indicative of the ionization energy (IE) of the species, while the shape of the PI curve lends clues to the geometry of any observed species.

Electronic structure calculations were carried out on the *Gaussian 09*^[13] computational chemistry software package. Two density functional theory (DFT) methods are selected for geometry optimizations and frequency calculations. The ubiquitous Becke three-parameter hybrid functional variation B3LYP with the Coulomb Attenuating Method (cam-B3LYP) is known to well account for long range interactions.^[14] The second functional used is the Minnesota functional M06-2X, a global hybrid functional well parameterized for main group non-metals with double the nonlocal exchange as M06.^[15] Frequency analysis is incorporated to confirm that each optimized structure is at a true local minimum on the potential energy surface. Both methods are used with the aug-cc-pVTZ basis set, i.e., Dunning's polarized correlation consistent triple-zeta basis set augmented with diffuse functions.^[16] The optimized structures are fed to CCSD(T)/aug-cc-pVTZ single point calculations in order to refine the energetics of the system at a high level of theory.^[17] Relative energetics are calculated as the sum of the electronic energy found at CCSD(T) and the zero-point energy from a given DFT. The CCSD(T) energies and DFT normal mode frequencies allow for calculation of the transition dipole moment and overlap integrals between neutrals and cations, which determines the progression of a simulated photoelectron spectrum (PES).^[18] These Franck-Condon simulations are then

integrated such that they are analogous to a photoionization spectrum.

Results and Discussion

Intense ion signals in the time-of-flight mass spectrum are observed at small flight times and constitute "turnaround" mass peaks, that is, ions that are heavy enough to have flight times so long that they appear early (or fast) in subsequent sweeps across the microchannel plate detector. The flight times of such turnaround ions are thus no longer meaningfully associated with the mass-to-charge ratio. This context arises in our study because the ion optics in the mass-spectrometer were optimized for a separate investigation of the reactivity of the methylidyne radical ($\text{CH}(X^2\Pi)$ for which bromoform serves as a radical precursor) towards other organic hydrocarbons, where the following discussion of tetrabromine is thus an unexpected yet exciting observation. Consequently, the mass spectrum does not extend beyond m/z 159. Despite lacking the m/z value of a given turnaround peak, the tunable ALS synchrotron radiation allows to collect a dependable PI curve to use for spectroscopic characterization. We thus first demonstrate this capability by the characterization of the reactant bromoform, CHBr_3 , as a turnaround cluster of intense peaks appearing at nominal m/z ratios between 4.5–6 amu. This section of the TOF-MS ion signal integrated across pre-photolysis times and over the full photon energy range of 8.4–10.75 eV is shown in Figure 1, in which the most intense cluster of peaks collected in our full dataset appears appear in a 1:3:3:1 ratio. This splitting in the time-of-flight is consistent with the isotopic abundance of a Br_n containing species of $n=3$. Additionally, small adjacent peaks mimicking the splitting but roughly 1.1% in relative intensity to the intense peaks are interspersed between and are easily assigned as the contribution from the corresponding ^{13}C -containing isotope combinations.

Identical photoionization spectra (Figure 2) are obtained for each individual peak in the TOF spectrum, the sum of which can be appropriately obtained by integrating over the full flight-time of the isotope cluster and the reaction time of 20 ms

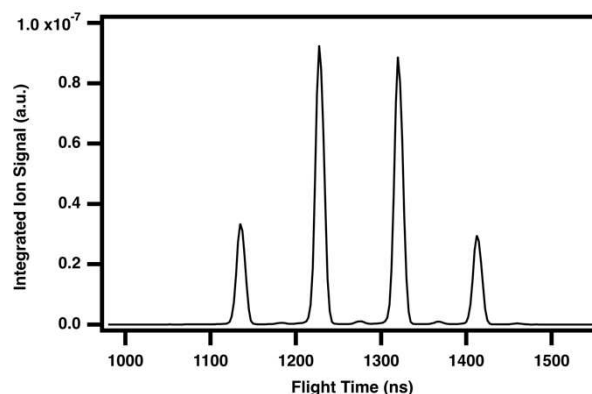


Figure 1. Photoionization time-of-flight mass spectrum of bromoform, CHBr_3 , integrated over 8.4–10.75 eV, 0–20 ms reaction time (pre-photolysis), and normalized to the photocurrent.

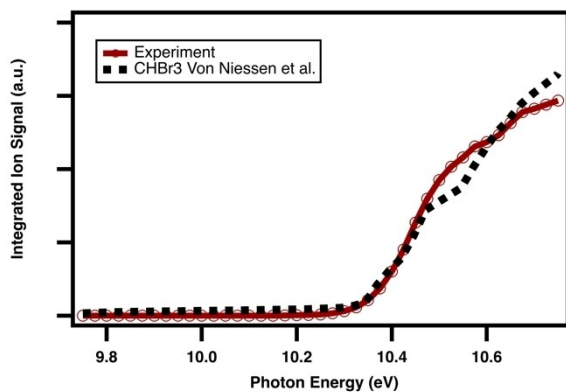


Figure 2. Observed mass-selected photoionization spectrum of bromoform, CHBr_3 , integrated over flight times of 1100–1500 ns, 0–20 ms reaction time (pre-photolysis), and normalized to the photocurrent (red with hollow circles). Reference photoelectron spectrum manually digitized and integrated from Von Niessen *et al.*^[19]

pre-photolysis (before the excimer laser starts firing). The experimental curve finds good agreement with the known photoelectron spectrum^[19] of CHBr_3 , from which integration yields an analogous PI spectrum for comparison to our collected signal.

Upon triggering of the reaction via the excimer photolysis laser, evidence of brominated reaction products is observed in the mass spectrum. Characterization of Br_2 is first achieved by identifying the peaks at m/z 79, 81, and 158. The range of the mass spectrum did not extend past m/z 159, and the isotopic peaks at m/z 160 ($^{79/81}\text{Br}_2$) and 162 ($^{81/81}\text{Br}_2$) are thus not observed. However, the isotopic distribution of Br_2 peaks would be expected to have a relative intensity of approximately 1:2:1. Molecular bromine is additionally known to have an auto-ionization fragment ion Br^+ (arising from an ion-pair process) of expected 1:1 relative intensities for m/z 79 and 81, as seen in Figure 3.^[20] We observe an ion signal of m/z 158 near 10.5 eV, matching the known ionization energy of Br_2 of 10.518 eV. The Br^+ fragment peaks at m/z 79 and 81 appear near 10.33 eV, in agreement with previous measurements.^[20–21] Any contribution

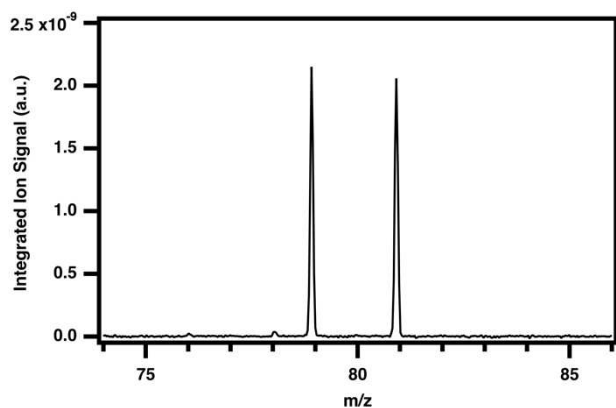


Figure 3. Photoionization time-of-flight mass spectrum of atomic bromine cation fragment, integrated over 8.4–10.75 eV, 0–100 ms reaction time, background subtracted, and normalized to the photocurrent.

to the ion signal originating from neutral atomic bromine at m/z 79/81 can be ruled out as it has an IE of 10.81 eV, which is above the photon energy scanned in this study.^[22]

Characterization is further verified by agreement between the respective photoionization spectra with literature plots in Figure 4.^[23] Additionally, the simulated photoelectron spectrum of Br_2 is integrated and included as a first test of the choice of computational methodology. Benchmarking both the camB3LYP and M06-2X functionals with Br_2 provides good agreement with established experimental results on structure and vibrational frequencies. Using the former method, error in the calculated Br–Br bond length is found to be 0.4%, with a deviation of 4.4% error from the established Br–Br stretch vibrational frequency, while for the Minnesota functional the percent errors are 0.2% and 6.3%, respectively. Single point energies are subsequently calculated at the *ab-initio* level CCSD(T)/aug-cc-pVTZ. The calculated adiabatic ionization (AIE) energy is taken as the energy difference of the zero-point corrected electronic energy of the cation and neutral ground state structures, respectively. Starting with either DFT functional before refining with CCSD(T) yields an AIE of 10.58 eV, which is 66 meV higher than the experimentally established IE of 10.52 eV by TPES.^[24]

A cluster of intense peaks are observed in the m/z 20–23 range of the mass spectrum and only grow in as post-photolysis signals. We believe these to be reaction products detected as turnaround peaks derived from two loosely tethered Br_2 molecules. The ion signal originating from a bromine-containing species of $n=4$ is hinted at through an observed isotopic distribution consistent with a corresponding expected 1:4:6:4:1 relative intensity of the integrated peak areas (Figure 5). Notably, in contrast to the CHBr_3 signal, this cluster of peaks shows no indication of a ^{13}C signal, and therefore is expected to be from a carbon free molecule with four bromine atoms. Identically shaped PI signals are obtained for each

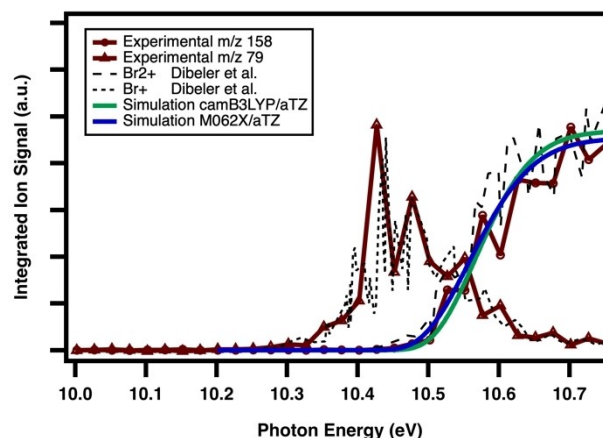


Figure 4. Observed mass-selected photoionization spectrum of molecular bromine integrated and background subtracted over 0–100 ms reaction time, and normalized to the photocurrent. Red with hollow circles is the observed m/z 158 curve, and red with solid triangles is the m/z 79 fragment PI curve. Reference threshold photoelectron spectrum manually digitized and integrated from Dibeler *et al.*^[23] of Br_2 and autoionization fragment Br (dashed black lines). Simulation of Br_2 at the camB3LYP/aug-cc-pVTZ (green) and M062X/aug-cc-pVTZ (blue) are superimposed onto as well.

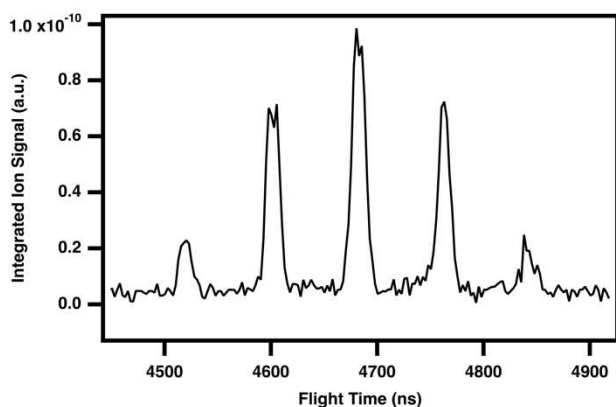


Figure 5. Photoionization time-of-flight spectrum of post-photolysis reaction product integrated over 8.4–10.75 eV, 0–100 ms reaction time with background subtraction, and normalized to the photocurrent.

isotopic peak, and the onset of the curve is observed at 10.2 eV with a sharp step-like transition. The PI spectrum's shape qualitatively indicates favorable Franck-Condon factors and is shown in Figure 6. In the case of Br_4 , geometries are taken from both Schuster *et al.*^[9] and Thanthiriwatte *et al.*^[10] Upon re-optimization of the D_{2h} geometry at the cam-B3LYP/aug-cc-pVTZ level, the cation shares the D_{2h} symmetry of the neutral cluster but with contracted bond lengths between both the two Br_2 subunits and within the Br_2 units themselves. This "square" configuration of two Br_2 subunits for both the neutral and cationic case is thus analogous to a homonuclear diatomic. Neither optimized structure possesses any calculated dipole moment, and both geometries are nonpolar. No successful optimization of the square D_{2h} geometry was found with M06-2X.

Conversely, starting with the L-shaped neutral, in which one Br_2 is colinear with one end of the other Br_2 , the cation equilibrates to a new configuration with the notable distortion being a break in symmetry from C_2 to C_1 , based on a dihedral

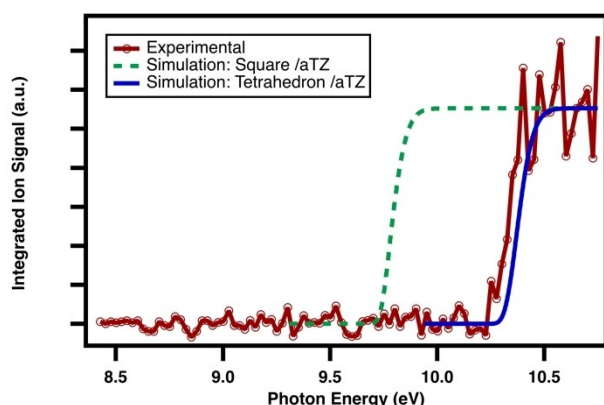


Figure 6. Observed mass-selected photoionization spectrum integrated over flight times of 4500–4900 ns, 0–100 ms reaction time and background subtracted, and normalized to the photocurrent. Observed PI curve (red with hollow circles), simulation of "square" geometry at camB3LYP/aug-cc-pVTZ (dashed green), and simulation of stretched tetrahedron geometry at M062X/aug-cc-pVTZ (solid blue).

angle change of 90 degrees such that the internuclear axis between each Br_2 moiety is approximately orthogonal. This is found to be the case using both functionals. Lastly, we consider the case of an elongated tetrahedral geometry not previously discussed in the literature. This local minimum is located with the M06-2X functional but did not converge in attempts using cam-B3LYP. Instead of two Br_2 in a planar configuration, one is rotated 90°. However, while forming a tetrahedron, the Br_2 – Br_2 distance is greater than each diatomic bond such that the symmetry is reduced from T_d to D_{2h} . A summary of the DFT optimized parameters, including geometries and harmonic vibrational frequencies, is provided in Table 1.

For each isomer considered, the adiabatic ionization energy is refined with CCSD(T) single point calculations. While the use of different functionals typically excludes direct comparison, the fact that the L-isomer is identically captured by both DFT levels allows for relative energetics to be qualitatively useful. Indeed, starting from the M06-2X optimized L-isomer, the single-point calculations find it is higher in both the case of the neutral and cation than the corresponding camB3LYP version by less than 2 meV, leading to an identical AIE also within 2 meV. A schematic energy level diagram is given in Figure 7.

Based on the sole existing claim of Br_4^+ as a polar ion in the gas phase (albeit with no other structural information), one is inclined to assume that the polar, twisted "L" structure is the dominant Br_4^+ conformer.^[8] Contrastingly, based on analogy with crystalline Cl_4^+ (and the dimerization of two I_2^+ ions, I_4^{2+}), the rectangular structures similarly appear likely.^[3a,6b] However, based on the calculated CCSD(T)/aug-cc-pVTZ AIE for each candidate alone, only the tetrahedron with an AIE of 10.31 eV is near the onset of the experimental spectrum. Both the tetrahedron and L-shaped neutral Br_4 are expected to be more thermodynamically favored than the square neutral by approximately 50 and 70 meV, respectively. Simulations are integrated and overlaid with the observed photoionization spectrum in

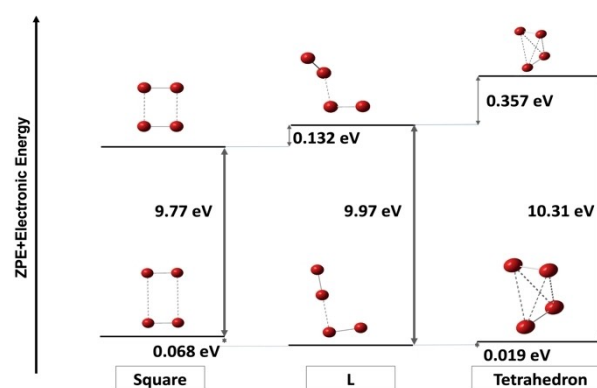


Figure 7. Energy level diagram of three considered Br_4 conformers. Geometry optimizations and frequency calculations are performed at camB3LYP/aug-cc-pVTZ for Square and L, with the energies taken as the sum of the CCSD(T)/aug-cc-pVTZ electronic energy and ZPE calculated at the DFT level. Geometry optimizations and frequency calculations are performed at M062X/aug-cc-pVTZ for L and Tetrahedron, with the energies taken as the sum of the CCSD(T)/aug-cc-pVTZ electronic energy and ZPE calculated at the DFT level. Note that the relative energetics for the L structure are identical across DFT methodologies at the reported precision.

Table 1. Optimized parameters for neutral and cationic Br₄ isomers: geometry labels; equilibrium bond lengths, R_e, in Å; bond angles in degrees, α; dihedral angle in degrees, γ; vibrational frequencies in wave-numbers cm⁻¹, ω.

CAM-B3LYP/aug-cc-pVTZ					
Geometry label	R _e	α	γ	ω	ZPE (meV)
L	2.297	101.52	–	4.83	48
	3.196			30.46	
	2.290			33.60	
				40.65	
				327.01	
L+	2.252	109.54	91.41	14.50	53
	3.017	109.54		33.56	
	2.252			36.59	
				104.15	
square	2.291	90.00	0.00	3.13	43
	4.817			4.35	
	4.817			10.04	
	2.291			12.21	
				333.14	
square+	2.239	90.00	0.00	30.47	57
	3.347			40.12	
	3.347			68.73	
	2.239			85.66	
				342.02	
M06-2X/aug-cc-pVTZ					
Geometry label	R _e	α	γ	ω	ZPE (meV)
L	2.291	88.37	–	39.09	56
	3.365			56.18	
	2.284			59.27	
				71.38	
				334.96	
L+	2.246	105.92	93.63	32.14	59
	2.997	105.92		51.86	
	2.246			57.22	
				117.35	
tetrahedron	2.282	–	84.75	50.79	59
	3.920			69.08	
	3.920			72.94	
	3.920			73.00	
	3.921			343.58	
tetrahedron+	2.282			344.16	
	2.336	–	84.28	39.78	56

Table 1. continued

CAM-B3LYP/aug-cc-pVTZ					
Geometry label	R _e	α	γ	ω	ZPE (meV)
	3.708			45.51	
	3.709			45.51	
	3.708			59.74	
	3.709			339.99	
	2.234			364.93	

Figure 6. Notably, the significant geometry difference of one Br₂ rotating out of plane in the L cation←neutral transition results in a near-zero overlap for the vibrational wavefunctions, a feature that is agnostic to the level of DFT employed and renders the simulation unreliable. This consequence extends to transitions between isomer pairs, and we predict no observable vertical transitions in mixed isomer pairs. While the square transition matches qualitatively in shape as a sharp rise to plateau, an unphysical energy shift of approximately +0.5 eV needs to be applied in order to find agreement with the observed PI spectrum. No significant shift is required in the case of the elongated tetrahedron. This close match in calculated AIE at the CCSD(T) level with the strong agreement in the shape of the spectrum provides evidence that the observed ion signal originates from a thermodynamically favorable tetrahedron-shaped Br₄ molecule formed as a recombination product during bromoform dissociation.

Conclusions

In summary, the Br₄⁺ ion is detected upon the photodissociation of bromoform using photoionization mass spectrometry coupled to tunable synchrotron radiation. This allows for a joint theoretical and experimental investigation resulting in the proposed structural characterization of Br₄ and Br₄⁺. Optimized bond parameters and vibrational frequencies are computationally determined with the coulomb-attenuating DFT method cam-B3LYP/aug-cc-pVTZ or M06-2X/aug-cc-pVTZ, and single point energetics are found with the *ab-initio* CCSD(T)/aug-cc-pVTZ level of theory in all cases. Simulating Franck-Condon overlap integrals allows for a theoretical photoelectron spectrum to be integrated and compared against the experimental photoionization spectrum. Results point to the formation of Br₄ in the gas-phase to have a distorted tetrahedral geometry of D_{2h} symmetry. Insights into the mechanism of Br₄ synthesis following initial bromoform photolysis in the gas phase is still unknown and a subject of further investigation.

Acknowledgements

This work was financially supported by the University of San Francisco (USF) Faculty Development Fund. The authors would like to acknowledge the Advanced Light Source (ALS) division

of the Lawrence Berkeley National Laboratory for beam time allocation at the 9.0.2 Chemical Transformations (VUV) Beamline, and Alexey Fedosov for the maintenance of the chemistry computer cluster at USF. The ALS is supported by the Director, Office of Science, Office of Basic Energy Sciences, of the U.S. Department of Energy under contract no. DE-AC02-05CH11231. The authors also express their gratitude to the Sandia National Laboratory teams led by Drs. Taatjes and Osborn for the utilization of the multiplexed synchrotron photoionization mass spectrometer, which is supported by the Division of Chemical Sciences, Geosciences and Biosciences, Office of Basic Energy Sciences (BES), US Department of Energy (USDOE).

Conflict of Interests

The authors declare no conflict of interest.

Data Availability Statement

The data that support the findings of this study are available from the corresponding author upon reasonable request.

Keywords: synchrotron photoionization · multiplexed mass spectrometry · adiabatic ionization energy · tetrabromine cluster · distorted tetrahedral D_{2h} structure

- [1] a) S. Brownridge, I. Krossing, J. Passmore, H. D. B. Jenkins, H. K. Roobottom, *Coord. Chem. Rev.* **2000**, *197*, 397–481; b) R. A. Garrett, R. J. Gillespie, J. B. Senior, *Inorg. Chem.* **1965**, *4*, 563–566; c) I. C. Tornieporth-Oetting, T. M. Klapötke, *Heteroat. Chem.* **1993**, *4*, 543–552.
- [2] a) H. Zhang, Z. A. Schelly, D. S. Marynick, *J. Phys. Chem. A* **2000**, *104*, 6287–6294; b) M. H. Whangbo, J. M. Williams, A. J. Schultz, T. J. Emge, M. A. Beno, *J. Am. Chem. Soc.* **1987**, *109*, 90–94; c) W. R. Simpson, R. von Glasow, K. Riedel, P. Anderson, P. Ariya, J. Bottenheim, J. Burrows, L. J. Carpenter, U. Frieß, M. E. Goodsite, D. Heard, M. Hutterli, H. W. Jacobi, L. Kaleschke, B. Neff, J. Plane, U. Platt, A. Richter, H. Roscoe, R. Sander, P. Shepson, J. Sodeau, A. Steffen, T. Wagner, E. Wolff, *Atmos. Chem. Phys.* **2007**, *7*, 4375–4418; d) S. C. Wofsy, M. B. McElroy, Y. L. Yung, *Geophys. Res. Lett.* **1975**, *2*, 215–218.
- [3] a) S. Seidel, K. Seppelt, *Angew. Chem. Int. Ed.* **2000**, *39*, 3923–3925; b) R. J. Gillespie, M. J. Morton, *Chem. Commun. (Camb.)* **1968**, 1565–1567; c) A. J. Edwards, G. R. Jones, *Journal of the Chemical Society A: Inorganic, Physical, Theoretical* **1971**, 2318–2320.
- [4] a) K. O. Christe, R. Bau, D. Zhao, *Z. Anorg. Allg. Chem.* **1991**, *593*, 46–60; b) A. J. Edwards, G. R. Jones, *Journal of the Chemical Society A: Inorganic, Physical, Theoretical* **1970**, 1891–1894; c) J. Passmore, G. Sutherland, P. S. White, *Inorg. Chem.* **1981**, *20*, 2169–2171; d) O. Glemser, A. Šmalc, *Angew. Chem. Int. Ed. Engl.* **1969**, *8*, 517–517.
- [5] a) K. C. Lee, F. Aubke, *Inorg. Chem.* **1980**, *19*, 119–122; b) H. Hartl, J. Nowicki, R. Minkwitz, *Angew. Chem. Int. Ed. Engl.* **1991**, *30*, 328–329; c) A. Apblett, F. Grein, J. P. Johnson, J. Passmore, P. S. White, *Inorg. Chem.* **1986**, *25*, 422–426.
- [6] a) R. J. Gillespie, J. B. Milne, M. J. Morton, *Inorg. Chem.* **1968**, *7*, 2221–2225; b) R. J. Gillespie, R. Kapoor, R. Faggiani, C. J. L. Lock, M. Murchie, J. Passmore, *J. Chem. Soc. Chem. Commun.* **1983**, 8–9.
- [7] T. Brichall, R. D. Myers, *J. Chem. Soc. Chem. Commun.* **1982**, 1174–1175.
- [8] K. V. Chance, K. H. Bowen, J. S. Winn, W. Klemperer, *J. Chem. Phys.* **1980**, *72*, 791–793.
- [9] P. Schuster, H. Mikosch, G. Bauer, *J. Chem. Phys.* **1998**, *109*, 1833–1844.
- [10] K. S. Thanthiruwatte, J. M. Spruell, D. A. Dixon, K. O. Christe, H. D. B. Jenkins, *Inorg. Chem.* **2014**, *53*, 8136–8146.
- [11] a) E. Carrasco, K. J. Smith, G. Meloni, *J. Phys. Chem. A* **2018**, *122*, 280–291; b) D. L. Osborn, P. Zou, H. Johnsen, C. C. Hayden, C. A. Taatjes, V. D. Knyazev, S. W. North, D. S. Peterka, M. Ahmed, S. R. Leone, *Rev. Sci. Instrum.* **2008**, *79*, 104103; c) M. Y. Ng, J. Nelson, C. A. Taatjes, D. L. Osborn, G. Meloni, *J. Phys. Chem. A* **2014**, *118*, 3735–3748.
- [12] a) W. S. McGivern, O. Sorkhabi, A. G. Suits, A. Derecskei-Kovacs, S. W. North, *J. Phys. Chem. A* **2000**, *104*, 10085–10091; b) P. Zou, J. Shu, T. J. Sears, G. E. Hall, S. W. North, *J. Phys. Chem. A* **2004**, *108*, 1482–1488.
- [13] M. J. Frisch, G. W. Trucks, H. B. Schlegel, G. E. Scuseria, M. A. Robb, J. R. Cheeseman, G. Scalmani, V. Barone, G. A. Petersson, H. Nakatsuji, X. Li, M. Caricato, A. V. Marenich, J. Bloino, B. G. Janesko, R. Gomperts, B. Mennucci, H. P. Hratchian, J. V. Ortiz, A. F. Izmaylov, J. L. Sonnenberg, Williams, F. Ding, F. Lipparini, F. Egidi, J. Goings, B. Peng, A. Petrone, T. Henderson, D. Ranasinghe, V. G. Zakrzewski, J. Gao, N. Rega, G. Zheng, W. Liang, M. Hada, M. Ehara, K. Toyota, R. Fukuda, J. Hasegawa, M. Ishida, T. Nakajima, Y. Honda, O. Kitao, H. Nakai, T. Vreven, K. Throssell, J. A. Montgomery Jr., J. E. Peralta, F. Ogliaro, M. J. Bearpark, J. J. Heyd, E. N. Brothers, K. N. Kudin, V. N. Staroverov, T. A. Keith, R. Kobayashi, J. Normand, K. Raghavachari, A. P. Rendell, J. C. Burant, S. S. Iyengar, J. Tomasi, M. Cossi, J. M. Millam, M. Klene, C. Adamo, R. Cammi, J. W. Ochterski, R. L. Martin, K. Morokuma, O. Farkas, J. B. Foresman, D. J. Fox, Wallingford, CT, **2016**.
- [14] T. Yanai, D. P. Tew, N. C. Handy, *Chem. Phys. Lett.* **2004**, *393*, 51–57.
- [15] Y. Zhao, D. G. Truhlar, *Theor. Chem. Acc.* **2008**, *120*, 215–241.
- [16] T. H. D. Jr, *J. Chem. Phys.* **1989**, *90*, 1007–1023.
- [17] G. D. Purvis III, R. J. Bartlett, *J. Chem. Phys.* **1982**, *76*, 1910–1918.
- [18] a) D. L. Baulch, C. T. Bowman, C. J. Cobos, R. A. Cox, T. Just, J. A. Kerr, M. J. Pilling, D. Stocker, J. Troe, W. Tsang, R. W. Walker, J. Warnatz, *J. Phys. Chem. Ref. Data* **2005**, *34*, 757–1397; b) T. A. Cool, A. McIlroy, F. Qi, P. R. Westmoreland, L. Poisson, D. S. Peterka, M. Ahmed, *Rev. Sci. Instrum.* **2005**, *76*, 094102; c) P. T. Ruhoff, *Chem. Phys.* **1994**, *186*, 355–374.
- [19] W. von Niessen, L. Åsbrink, G. Bieri, *J. Electron Spectrosc. Relat. Phenom.* **1982**, *26*, 173–201.
- [20] J. D. Morrison, H. Hurzeler, M. G. Inghram, H. E. Stanton, *J. Chem. Phys.* **1960**, *33*, 821–824.
- [21] a) K. Watanabe, *J. Chem. Phys.* **2004**, *26*, 542–547; b) D. C. Frost, C. A. McDowell, *Can. J. Chem.* **1960**, *38*, 407–420.
- [22] K. Kimura, T. Yamazaki, Y. Achiba, *Chem. Phys. Lett.* **1978**, *58*, 104–107.
- [23] V. H. Dibeler, J. A. Walker, K. E. McCulloh, *J. Chem. Phys.* **1970**, *53*, 4715–4716.
- [24] A. J. Yencha, A. Hopkirk, A. Hiraya, R. J. Donovan, J. G. Goode, R. R. J. Maier, G. C. King, A. Kvaran, *J. Phys. Chem.* **1995**, *99*, 7231–7241.

Manuscript received: November 13, 2023

Revised manuscript received: January 22, 2024

Version of record online: February 2, 2024